applied sciences

MDPI

Article

Detecting and Evaluating Displacements of Paving Blocks Adjacent to Deep Excavation Sites Using Terrestrial Photogrammetry

Taesik Kim [1], Ho Choi [2], Jinman Jung [3], Hong Min [4,*] and Young-Hoon Jung [5,*]

[1] Department of Civil Engineering, Hongik University, Seoul 04066, Republic of Korea; taesik.kim@hongik.ac.kr
[2] Department of Urban Infrastructure Research, Seoul Institute of Technology, Seoul 03909, Republic of Korea; choiho@sit.re.kr
[3] Department of Computer Engineering, Inha University, Incheon 22212, Republic of Korea; jmjung@inha.ac.kr
[4] School of Computing, Gachon University, Seongnam 13120, Republic of Korea
[5] Department of Civil Engineering, Kyung Hee University, Yongin-si 17104, Republic of Korea
* Correspondence: hmin@gachon.ac.kr (H.M.); jyounghoon@khu.ac.kr (Y.-H.J.)

Featured Application: The terrestrial photogrammetry technique provides an efficient and accurate solution for evaluating ground deformations induced by construction activities.

Abstract: In urban areas, deep excavation-induced ground deformations may damage adjacent existing structures and are conventionally evaluated by levelling at installed settlement points. However, a small number of measurements cannot represent the total changes in ground deformations adjacent to excavation sites. Furthermore, significant local subsidences may occur in places where settlement points have not been installed and only noticed after an accident. For deep excavation sites located in urban areas, paved pedestrian sidewalks are often located adjacent to sites, and construction activities can cause these paving blocks to become displaced. This study introduces a method to detect paving block displacements adjacent to deep excavation sites using terrestrial photogrammetry. A digital camera creating point cloud data (PCD) and an acquisition method satisfying the frontal and side overlap requirements were demonstrated. To investigate the displacement detections and measurement capabilities by PCD analysis, an experimental program was conducted, including a PCD comparison containing the uplift, settlement, and horizontal paving block displacement and reference data. The cloud-to-cloud distance computation algorithm was adopted for PCD comparisons. Paving block displacements were detected for displacements of 5, 7.5, and 10 mm in the uplift, settlement, and horizontal directions; however, the horizontal displacements were less clear. PCD analysis enabled satisfactory measurements between 0.024 and 0.881 mm for the vertical-displacement cases, but significant errors were observed for the horizontal-displacement cases owing to the cloud-comparison algorithm. The measurement blind spot of limited settlement points was overcome by the proposed method that detected and measured paving block displacements adjacent to excavation sites.

Keywords: terrestrial photogrammetry; deep excavation; paving block; displacement detection

Citation: Kim, T.; Choi, H.; Jung, J.; Min, H.; Jung, Y.-H. Detecting and Evaluating Displacements of Paving Blocks Adjacent to Deep Excavation Sites Using Terrestrial Photogrammetry. *Appl. Sci.* **2023**, *13*, 7245. https://doi.org/10.3390/app13127245

Academic Editor: Laurent Daudeville

Received: 9 May 2023
Revised: 6 June 2023
Accepted: 13 June 2023
Published: 17 June 2023

1. Introduction

Recent emphasis on serviceability control in geotechnical engineering projects demands accurate measurements of the displacements of structures and the ground surface. Numerous studies have been conducted to analyze the factors affecting the ground deformation during deep excavation, whether in rock or soil [1–7]. Routine measurements of ground settlements adjacent to a deep excavation project are legally mandated, although only a minimum number of monitoring points are controlled in most projects with tight

budgets. Unfortunately, such legal efforts have not successfully prevented a catastrophic collapse, mainly because the location initiating the collapse is often out of the range controlled by the measurement of the monitoring points. The adaptive management technique for ground deformation control including the inverse analysis is also limited because it relies on those monitoring points [8,9]. Settlement measurements are possible with synthetic-aperture radar (SAR), but images of the area of interest may be insufficient for frequent investigation [10]. Consequently, a technique for measuring the displacements induced by excavation work in the entire range or full field is crucial for ensuring construction safety [11].

Recent developments in computer performance and the increased use of digital photographs have stimulated advances in photogrammetric software. Photogrammetry is a technique for determining the three-dimensional geometry of physical objects by measuring and analyzing their two-dimensional photographs. Terrestrial photography provides detailed dimensional information about an object using images near or on the surface of the earth. In close-range terrestrial photography, the size of the object and the camera-to-object distance are both less than 100 m [12]. Several papers related to close-range photogrammetry have been dedicated to various application fields such as industrial engineering [13], cultural heritage documentation [14–18], and geomorphology [19–23]. Close-range terrestrial digital photogrammetry is widely applied in rock mass discontinuity characterization [24]. In civil engineering, close-range photogrammetry plays a vital role in engineering surveys, including as-built documentation of existing facilities and building information modeling. The bridge deformation and health monitoring were measured using the photogrammetry technique [12,25–29]. The deformation of concrete tanks and retaining walls under working conditions can be measured using high-precision photogrammetry with high-resolution cameras [30,31].

Various applications of the close-range terrestrial photogrammetry technique also reveal the possibility of full-field measurements of displacements induced by deep excavation work in urban areas. Pedestrian sidewalks paved with concrete pavement blocks are frequently located adjacent to deep excavation sites. Measuring the displacements of these pavement or paving blocks via close-range photogrammetry can resolve the practical difficulties in investigating the ground deformation induced by deep excavation works in urban areas. We opted to use Unmanned Ground Vehicles (UGVs) as an alternative to Unmanned Aerial Vehicles (UAVs), as the latter often lead to safety and regulatory concerns when operated in urban areas [32–36].

To the extent of our understanding, the methodology of monitoring the movements of paving blocks through close-range photogrammetry, carried out by cameras affixed to the UGV system, has not been systematically presented. Figure 1 displays the paving blocks adjacent to the excavation site. In Figure 1, the construction site is located behind the wall; moreover, various displacements of paving blocks can be observed.

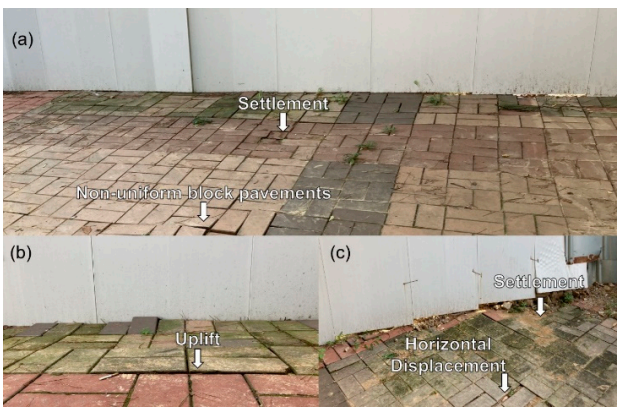

Figure 1. Displacements of paving blocks adjacent to the deep excavation site: (**a**) settlement and non-uniform block pavements; (**b**) uplift; and (**c**) settlement and horizontal displacement.

This study introduces a workflow for detecting the displacements of paving blocks adjacent to deep excavation sites. This workflow mainly relies on close-range terrestrial photogrammetry and structure-from-motion (SfM) photogrammetric techniques. The requirements for establishing reliable point cloud data (PCD) for paving blocks including ground sampling distance, image network geometry, and parameters of the camera mounted on an unmanned ground vehicle (UGV) are presented. The applicability of the cloud-to-cloud (C2C) distance computation algorithm is discussed to trace temporal changes in the uplift, settlement, and horizontal movement of paving blocks.

2. Materials and Methods

Figure 2 illustrates a flowchart of the proposed methodology. It shows the flow of the digital image acquisition method, PCD creation using digital images, and displacement detection and measurement through PCD comparison. The details of individual items in the flowchart are presented in the following sections.

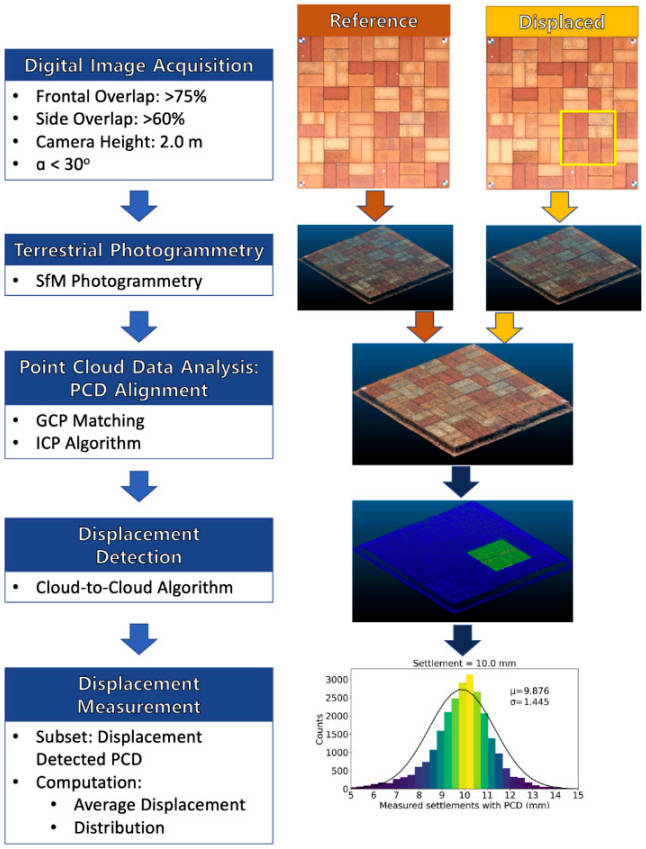

Figure 2. Flowchart of the proposed methodology. Blocks inside the yellow box were displaced.

2.1. Digital Image Acquisition

A camera was selected to move the UGV in a paving block adjacent to the excavation site. The camera must be lightweight, capable of continuous shooting for photogrammetry, and able to obtain stable images without shaking. An action camera (GoPro HERO7 Black) was used to obtain digital images for terrestrial photogrammetry. Action cameras specialize in recording smooth videos while moving. It may not need a gimbal, but using a gimbal makes it easy to adjust the angle of viewing and can also provide auxiliary stabilization. The GoPro HERO 7 Black weighs 116 g, and the Feiyu WG2X gimbal used weighs 238 g. If a digital single-lens reflex camera was employed for image acquisition, the total weight would be greater than 3 kg. This is approximately ten times heavier than that of the action camera system, and therefore, the UGV would be inefficient as more energy is used to move.

To obtain digital images for terrestrial photogrammetry, it is necessary to evaluate the ground sample distance (GSD), which is the distance between the pixel centers measured on the ground and the field of view (FOV) according to the camera shooting height. For the employed camera, the width of the charge-coupled device was 6.17 mm with 4096 pixels, and the horizontal FOV was 86°. As shown in Figure 3a, the GSD increased with the camera shooting height, and was less than 0.911 mm when the shooting height was lower than 2.0 m. The GSD value appeared to be sufficient to evaluate the paving block displacements adjacent to the excavation sites. The maximum shooting height was set to be 2.0 m.

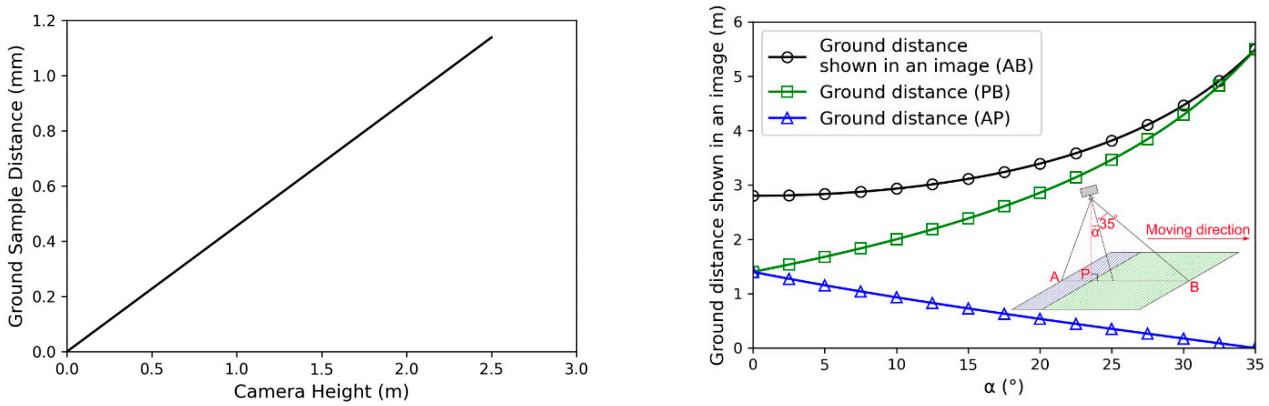

Figure 3. (**a**) Ground sample distance with camera height. (**b**) Ground distance shown in an image with α.

Figure 3b demonstrates the ground distances depicted in an image with a pitch angle (α) while the camera is positioned at a height of 2.0 m. In this scenario, the camera is mounted in a manner where it faces downwards, and the top of the image corresponds to the front direction. Half of the vertical FOV of the camera was 35°. When α is greater than 0°, the image becomes oblique, so it shows more of the ground in the travel direction. The ground distance PB shown in Figure 3b increases rapidly with increasing α, increasing the ground distance AB. However, the distance AP decreases. As a result, information far from the camera's position can be included in the image with a large α, making it difficult to properly create PCD. Consequently, a low-oblique image closer to a vertical image or vertical image was adopted to create PCD, rather than the high-oblique images. This is consistent with the recommendations of the SfM software manual that the camera should be kept as constant as possible over the terrain to ensure the desired GSD. The Pix4D mapper version 4.8.1 was used for the SfM software in this study.

To create a PCD, the recommended frontal overlap between the images should be at least 75%. The camera employs two methods to obtain digital images: capturing a snapshot with time lapse and extracting a frame from a video. The minimum interval between images is 0.5 s for time lapse. For frame extraction from a video at 30 fps, 30 images can be obtained in 1 s; therefore, the time interval between two consecutive images is 0.033 to 1 s. Note that digital images are obtained while moving on the sidewalk; therefore, moving at a high speed is dangerous for pedestrians. Accordingly, the practical moving speed range for image acquisition is 2.0 m/s or less, which is a typical jogging speed. As can be seen in Figure 4, the frontal overlap is affected by the movement speeds and α. If the moving speed is fast, it may not be possible to obtain a sufficient number of images that satisfy the 75% minimum frontal overlap recommended for photogrammetry [37]. When the moving speed was 1.0 m/s, frontal overlap could be satisfied with both image acquisition methods, as shown in Figure 4a. However, when the moving speed was 2.0 m/s, as indicated in Figure 4b, only the frame extraction whose interval was shorter than 0.33 s could satisfy the required frontal overlap, regardless of α. The method of capturing a snapshot with time lapse cannot satisfy the requirement when α is smaller than or equal to 25°; only the case

of $\alpha = 30^{\circ}$ can satisfy the requirement. Consequently, a method of extracting frames from videos was selected to obtain sufficient images for PCD creation.

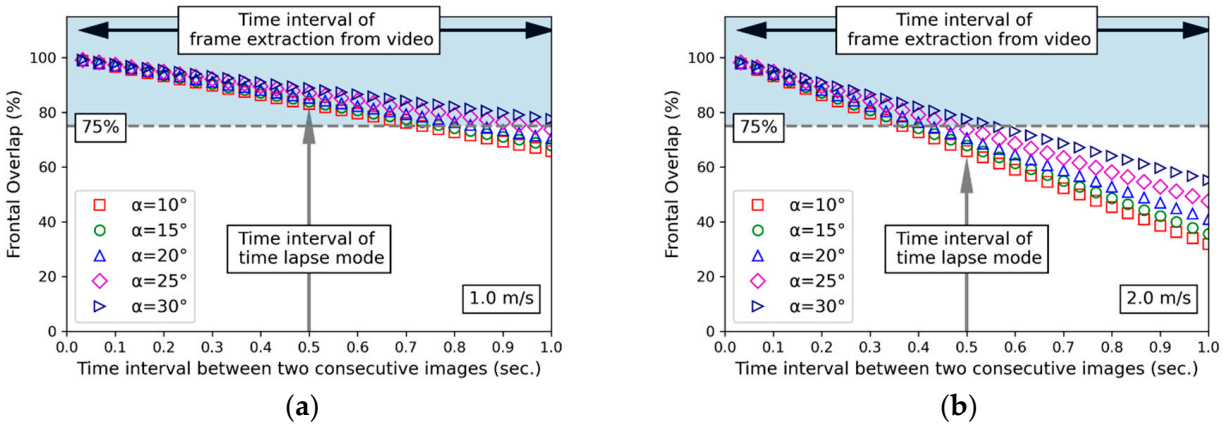

Figure 4. Frontal overlap depending on the time interval between two consecutive images with the moving speeds of (**a**) 1.0 m/s and (**b**) 2.0 m/s.

For a side overlap, the spacing between moving tracks is important to satisfy the requirement of at least 60% [37]. As shown in Figure 5, when the spacing was shorter than approximately 1.5 m, the required overlap was satisfied. Accordingly, the spacing was set shorter than 1.5 m when obtaining the images. Note that the camera was maintained at a constant shooting height of 2.0 m.

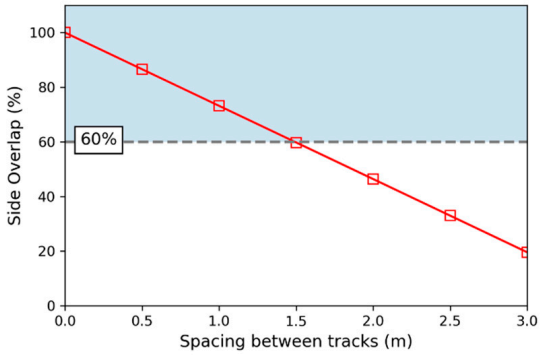

Figure 5. Side overlap versus distance between tracks.

2.2. Testing Program

In urban areas, existing buildings are often demolished and new buildings are constructed. In this case, the sidewalk adjacent to the excavation site used before construction continues to be used. Accordingly, ground movement adjacent to the excavation site causes displacements of the paving blocks. In this study, three cases of paving block movements that can be found in Figure 1 were evaluated: uplift, settlement, and horizontal displacement. Evaluations were performed at 5 mm, 7.5 mm, and 10 mm in each case.

Figure 6 shows the reference without displacement setup to detect and measure the movements of the paving blocks measuring 1380 cm × 1380 cm. Seventy-two paving blocks with dimensions of 230 mm × 115 mm × 60 mm were used. The four corner markers were ground control points (GCPs), where the coordinates were measured using a global navigation satellite system rover, Trimble R10. These GCPs were utilized for the georeferencing of the PCD. By adding geographic information to the image, it is easy to detect and calculate changes in the PCD. The uplift and horizontal displacement of the paving block were induced by installing spacers in the reference paving block setup. Settlement was created by lowering the level of the floor where the paving block was placed.

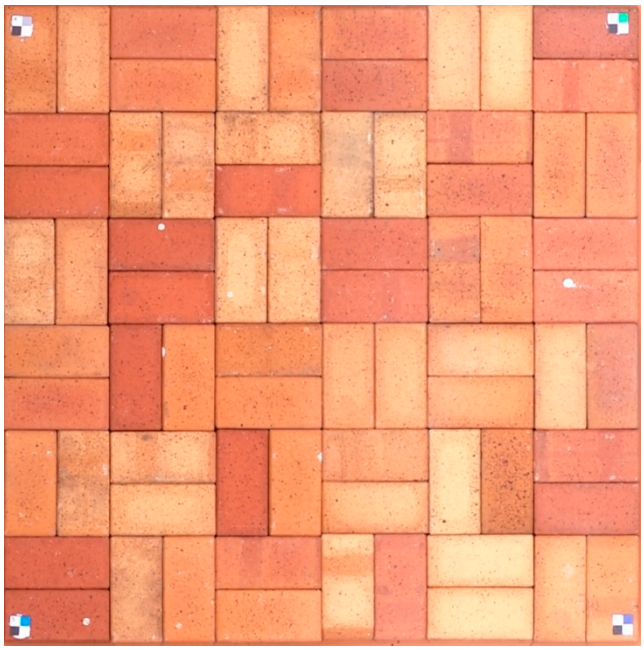

Figure 6. Reference set up for paving blocks for the detection and measurement of block displacements.

For each test setup, two round-trip videos were recorded using GoPro 7 Hero Black, and the frames extracted from the videos were used for PCD creation. In a single round trip, videos were recorded along the same track at a height of 2 m. The distance between the tracks was within 1.5 m to satisfy the side-overlap requirement. The PCD was created using a Pix4D mapper.

2.3. Data Interpretation

PCD with various displacements, PCDd, were compared with the reference PCD, PCDr. The open-source software CloudCompare version 2.12.4 was used for point cloud processing. Since identical GCPs were used for the creation of the PCD, the PCD were well aligned during the comparison. For better results, PCDd was slightly rotated and translated to fit PCDr using the iterative closest point (ICP) algorithm. Note that the ICP algorithm can minimize the difference between two PCD and is often used to construct a single PCD from different scans in several engineering fields. The displaced paving blocks were excluded while the ICP algorithm optimized the transformation matrix to determine the best fit, because the displaced paving blocks would influence matrix optimization. After obtaining the optimized transformation matrix, it was applied to the paving blocks with displacements. By conducting this process, it was possible to precisely align the PCD.

The C2C algorithm was used to compare PCDd with PCDr. It calculates the distance between two PCD by simply determining the nearest neighbor distance between points. After calculation using the C2C algorithm, the points in the zones where the displacement occurrence was detected were subset. For this subset, the mean and standard deviation of the displacements were calculated, and the distribution was analyzed using a histogram.

3. Results and Discussion

3.1. Vertical Displacements

For the investigation of uplift cases, eight paving blocks were lifted by 5, 7.5, and 10 mm. As shown in Figures 7–9, it was possible to detect every tested uplift case. Note that blue indicates no displacement and green indicates displacement. The number of subset points where displacements occurred was approximately between 25,000 and 30,000. As indicated in the subfigures (d) of Figures 7–9, it can be seen that the distribution of displacements appears close to the normal distribution. When the accuracy was evaluated

by subtracting the actual uplift value from the mean value (μ) measured by the PCD, the tested cases of 5, 7.5, and 10 mm were 0.241, 0.074, and 0.080 mm, respectively. Herein, the standard deviation (σ) of the PCD measurements was regarded as precision. The precisions for the tested cases of 5, 7.5, and 10 mm were 0.930, 0.939, and 1.003 mm, respectively.

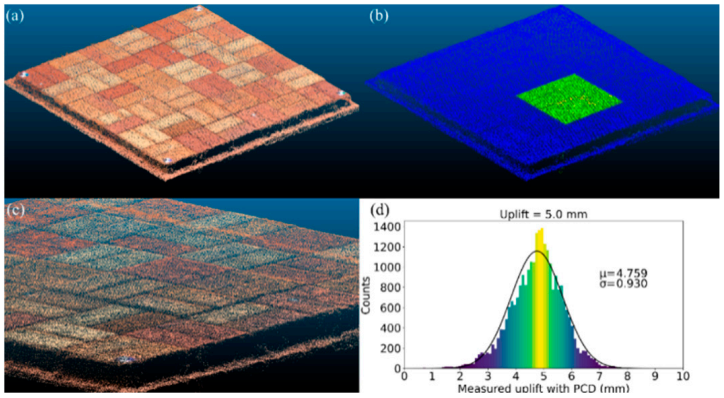

Figure 7. PCD of 5.0 mm uplift: (**a**) PCD; (**b**) visualization of the uplifted zone; (**c**) zoomed in the 5.0 mm uplifted zone; (**d**) histogram of the uplifted zone.

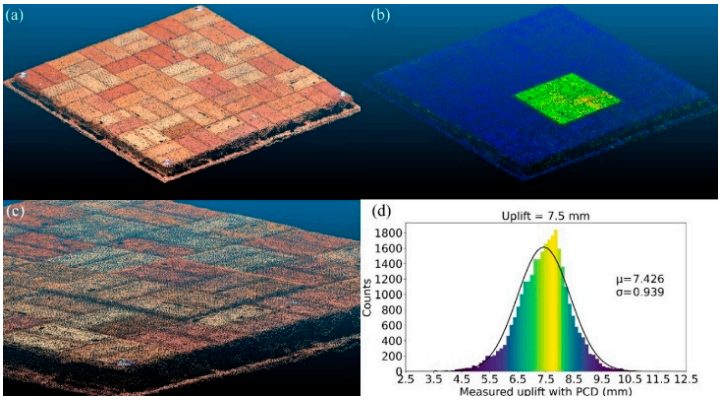

Figure 8. PCD of 7.5 mm uplift: (**a**) PCD; (**b**) visualization of the uplifted zone; (**c**) zoomed in the 7.5 mm uplifted zone; (**d**) histogram of the uplifted zone.

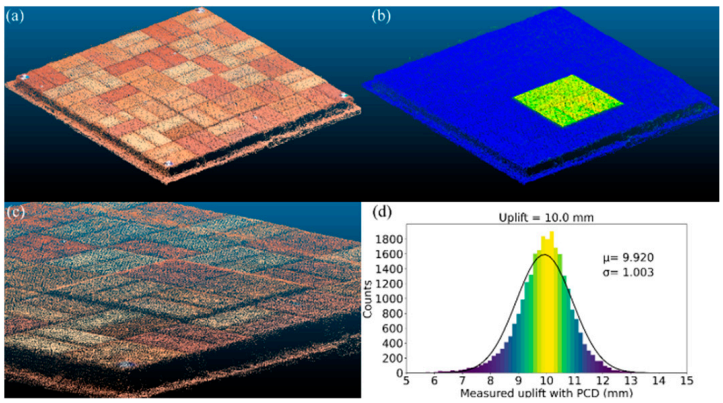

Figure 9. PCD of 10.0 mm uplift: (**a**) PCD; (**b**) visualization of the uplifted zone; (**c**) zoomed in the 10 mm uplifted zone; (**d**) histogram of the uplifted zone.

To investigate the settlement of the paving blocks, eight paving blocks were set to 5, 7.5, and 10 mm. As displayed in Figures 10–12, it is possible to detect every tested case. Since the C2C algorithm calculates the distance to the nearest point between PCD, information about directionality, such as settlement and uplift, is unknown. Similar to the

investigated uplift cases, blue indicates no displacement, and green indicates displacement. The number of subset points where displacements occurred was approximately between 25,000 and 30,000. As shown in the histogram of each case, the distribution was close to the normal distribution like the uplift cases. The mean values of the PCD measurements for the three cases were 5.881, 7.468, and 9.876 mm, respectively. When the accuracies were evaluated as in the uplift cases, the accuracies of the 5, 7.5, and 10 mm cases were 0.881, 0.032, and 0.024 mm, respectively. In addition, the standard deviations of three cases were 1.672, 1.231, and 1.445 mm for cases of 5, 7.5, and 10 mm, respectively.

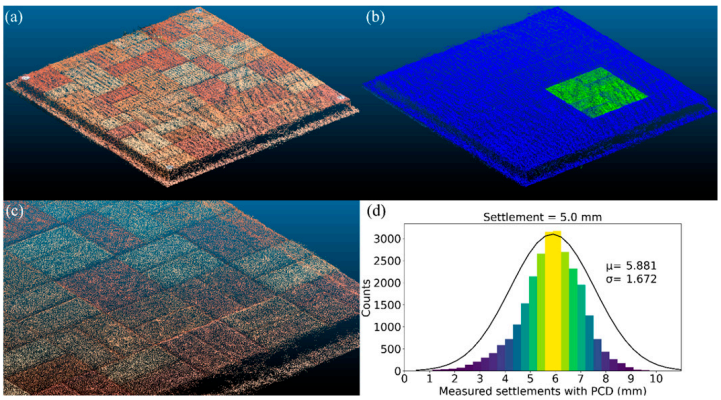

Figure 10. PCD of the 5.0 mm settlement: (**a**) PCD; (**b**) settled zone visualization; (**c**) zoomed in the 5.0 mm settled zone; (**d**) histogram of the settled zone.

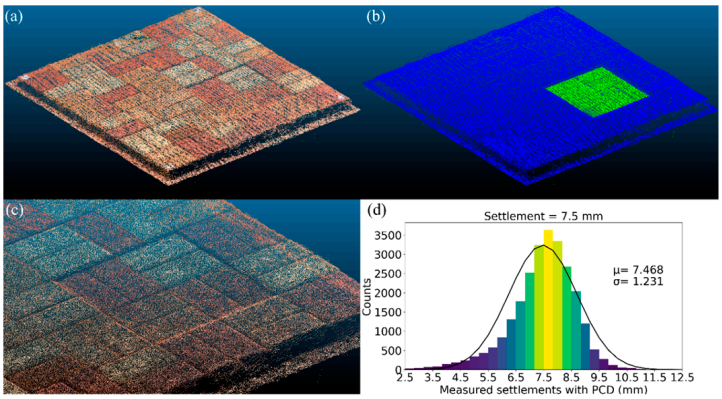

Figure 11. PCD of the 7.5 mm settlement: (**a**) PCD; (**b**) settled zone visualization; (**c**) zoomed in the 7.5 mm settled zone; (**d**) histogram of the settled zone.

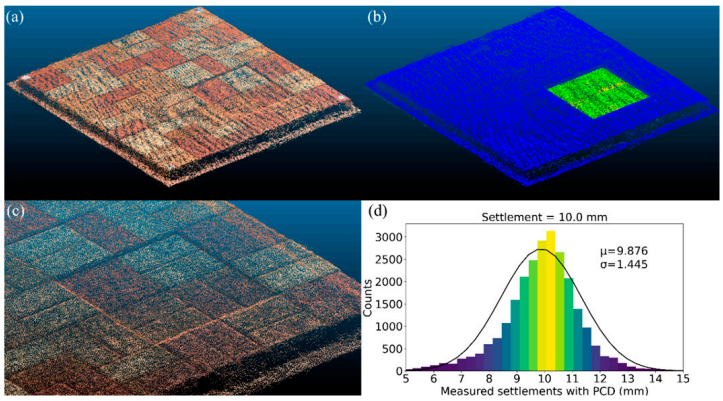

Figure 12. PCD of the 10.0 mm settlement: (**a**) PCD; (**b**) settled zone visualization; (**c**) zoomed in the 10.0 mm settled zone; (**d**) histogram of the settled zone.

Conventionally, the vertical displacement is evaluated by the level instrument at the installed settlement point; therefore, information about only that point can be obtained. However, the advantage of the level instrument is that it can measure a vertical displacement of 5 mm or less, which has not been tested here. Note that the standard deviation for the 1 km double-run levelling of these instruments is approximately 1 or 2 mm, as evaluated by ISO 17123-2 [38]. Based on the cases investigated using terrestrial photogrammetry, it can be inferred that it was possible to detect a vertical displacement of more than 5 mm. Vertical displacement evaluation using PCD is a measurement of a surface, and not a single point. Accordingly, it has the advantage of being able to determine displacements that would not have been known if there were no settlement points for the level instrument. From this point of view, PCD measurements seem to be sufficiently valuable for evaluating the vertical displacements adjacent to a deep excavation site. If the vertical displacement of the ground adjacent to the construction site is measured at the levelling error level, it is also possible to perform displacement detection using PCD and apply the level measurement to the area where displacements occur.

3.2. Horizontal Displacements

To investigate the horizontal displacements of the paving blocks, six blocks were horizontally displaced by 5, 7.5, and 10 mm, respectively. As demonstrated in Figure 13, it was possible to detect all the investigated cases, but the horizontal displacement of 5 mm was not clear, compared with the other cases. Overall, the horizontal displacement cases were not clearly visible compared with the vertical displacement. Note that blue indicates no displacement and green indicates displacement. Since the displacement zone is narrow, the number of subset points is approximately 1000, which is only 4% of that of the vertical cases. If the number of detected displaced points is small, the visibility may be poor.

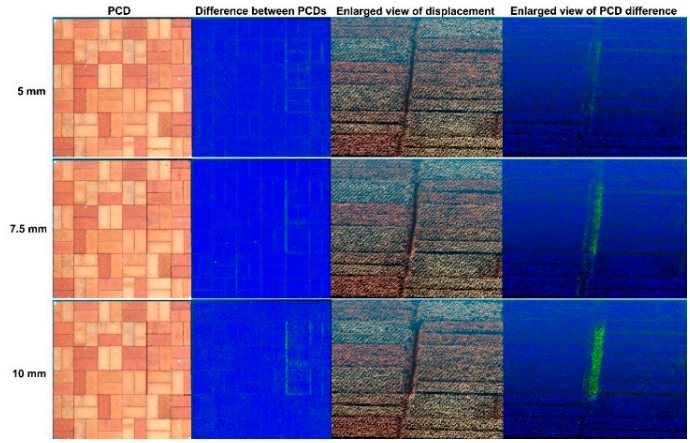

Figure 13. PCD analysis results of the horizontal displacement cases of 5 mm, 7.5 mm, and 10 mm.

As shown in Figure 14, the histogram of each case was close to the normal distribution, but the histogram bars were jagged compared with the vertical cases. The mean values of the PCD measurements for the 5, 7.5, and 10 mm displacement cases were 2.260, 3.614, and 6.225 mm, respectively. Clearly, the differences between the actual displacement value and mean were large, and the counts were very small at the actual displacements. Although horizontal displacements can be detected, the measurement errors are significant.

To determine why the measurement errors in the horizontal displacements were large compared with the vertical cases, further investigation was performed on the horizontal displacement cases. Figure 15 shows the PCD of the reference and investigated cases of a 10 mm horizontal displacement. Note that only a portion was extracted from the PCD for better presentation. The small dent shown in Figure 15a represents the chamfers of two closely adjoining paving blocks. Figure 15b indicates the PCD when one of the two adjacent paving blocks is horizontally separated by 10 mm, and the two PCD are plotted

together in Figure 15c. In Figure 15d, the color of PCDd is expressed using the calculated distance from PCDr instead of actual color information obtained from the digital image, and the distance scale is shown in the color bar. As previously noted, the algorithm used to compare PCDd with PCDr was C2C, which calculates the distance between two PCD. Since the algorithm simply computes the distance between the nearest neighbor points, the calculated distance does not represent the horizontal displacement; rather, it is closer to the vertical distance. Thus, it only provides scalar information and not vectors. Additionally, it cannot be concluded whether the vertical displacement is a rise or subsidence based on the computation results alone. When a displacement is detected, it is necessary to compare the PCD in the corresponding area.

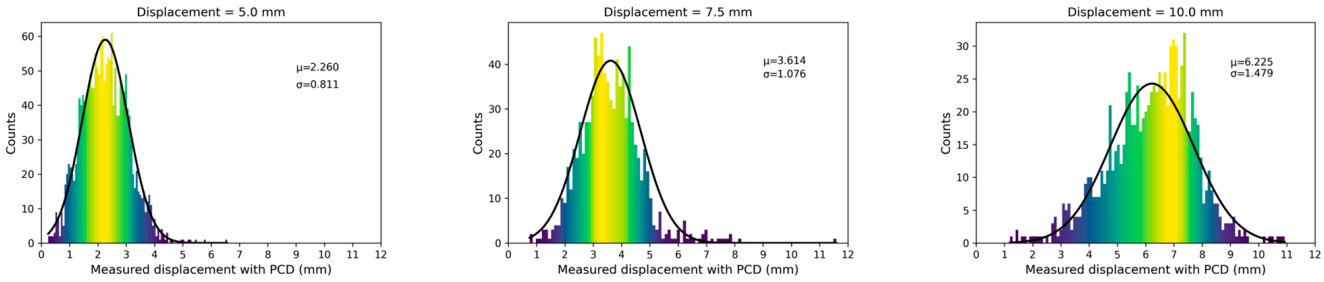

Figure 14. Histogram of investigated horizontal displacement cases: (**a**) 5 mm; (**b**) 7.5 mm; (**c**) 10 mm.

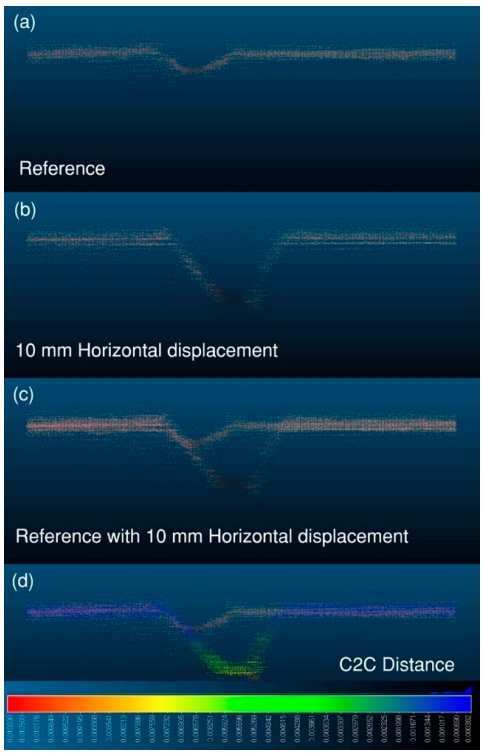

Figure 15. PCD of the reference and investigated cases for 10 mm horizontal displacement: (**a**) reference; (**b**) 10 mm horizontal displacement; (**c**) reference with 10 mm horizontal displacement; and (**d**) C2C distance.

Figure 16 shows an enlarged view of the area where the 10 mm horizontal displacement occurred. As can be seen in Figure 16, a 10 mm displacement could be found from the PCDd with the actual color. In addition, it was not easy to determine the difference from Figure 16b. However, it was shown that the green lines parallel to the slit were found to the right of the 10 mm displacement in Figure 16c, and the PCD was expressed using the

calculated distance from PCDr. This is because the paving blocks on the right side of the slit moved to the right when the spacing was 10 mm. When paving blocks are horizontally displaced, this pattern is expected to be found in the field.

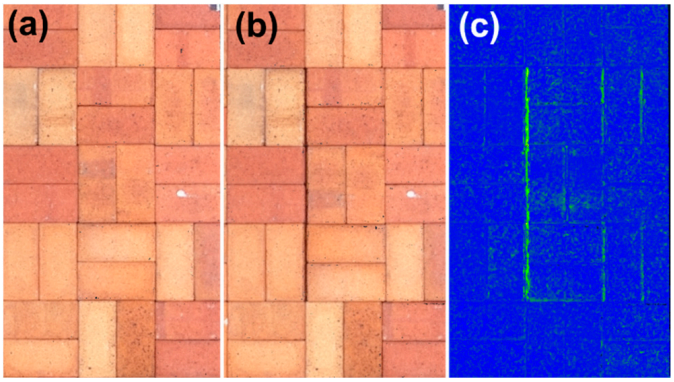

Figure 16. Enlarged views of the area with 10 mm horizontal displacement: (**a**) before displacement occurred; (**b**) after 10 mm displacement; (**c**) differences between PCD.

4. Conclusions

The close-range terrestrial photogrammetry technique was applied to measure the displacements of paving blocks, indicating the ground movement caused by deep excavation works. Sequential sets of PCD were generated using Pix4D software version 4.8.1 with SfM photogrammetry. The workflow for measuring temporal changes in the displacements of the paving blocks by computing the PCD sets is provided. The requirements of the photogrammetric technique, such as ground sampling distance, image network geometry, and camera parameters, were presented to obtain reliable point-cloud data.

Vertical displacements of the paving blocks exceeding 5 mm could be detected through the workflow using the C2C algorithm. However, the detection of the horizontal displacements was less successful than that of the vertical displacements, possibly because of the theoretical limit of the adopted C2C algorithm. The measurement accuracy of the proposed workflow can be improved by introducing a vector-based algorithm to compare PCD sets.

Author Contributions: Conceptualization, T.K. and Y.-H.J.; methodology, T.K.; software, J.J.; validation, H.C., J.J. and H.M.; formal analysis, H.C. and H.M.; investigation, H.C.; resources, H.M.; data curation, J.J.; writing—original draft preparation, T.K. and H.C.; writing—review and editing, Y.-H.J. and J.J.; visualization, T.K. and H.C.; supervision, Y.-H.J. and H.M.; project administration, Y.-H.J. and H.M.; funding acquisition, Y.-H.J. All authors have read and agreed to the published version of the manuscript.

Funding: This work was supported by a grant (No. 22SCIP-C151582-04) from the Construction Technologies Program funded by the Ministry of Land, Infrastructure and Transport of the Korea government and the National Research Foundation of Korea (NRF) grant funded by the Korea government (MSIT) (No. 2019R1A2C1089155). This work was also supported by Inha University Research Grant.

Institutional Review Board Statement: Not applicable.

Informed Consent Statement: Not applicable.

Data Availability Statement: Data available on request from the authors. The data that support the findings of this study are available from the corresponding author, Y.-H.J., upon reasonable request.

Conflicts of Interest: The authors declare no conflict of interest.

References

1. Zhao, Y.; Liu, Q.; Zhang, C.; Liao, J.; Lin, H.; Wang, Y. Coupled seepage-damage effect in fractured rock masses: Model development and a case study. *Int. J. Rock Mech. Min. Sci.* **2021**, *144*, 104822. [CrossRef]
2. Wu, H.; Jia, Q.; Wang, W.; Zhang, N.; Zhao, Y. Experimental test on nonuniform deformation in the tilted strata of a deep coal mine. *Sustainability* **2021**, *13*, 13280. [CrossRef]
3. Yu, W.; Liu, Z.; An, B.; Wang, P.; Wu, H. Mechanical characteristics and deformation control of surrounding rock in weakly Cemented Siltstone. *Environ. Earth Sci.* **2021**, *80*, 337. [CrossRef]
4. Yuan, Z.; Zhao, J.; Li, S.; Jiang, Z.; Huang, F. A unified solution for surrounding rock of roadway considering seepage, dilatancy, strain-softening and intermediate principal stress. *Sustainability* **2022**, *14*, 8099. [CrossRef]
5. Liu, J.; Tan, T.; Zhang, L.; Zhu, S.; Xu, F. Evolution and modeling of mine water inflow and hazard characteristics in southern coalfields of China: A case of Meitanba mine. *Int. J. Min. Sci. Technol.* **2022**, *32*, 513–524. [CrossRef]
6. Kim, T.; Finno, R. Anisotropy evolution and irrecoverable deformation in triaxial stress probes. *J. Geotech. Geoenviron. Eng.* **2012**, *138*, 155–165. [CrossRef]
7. Finno, R.; Kim, T. Effects of stress path rotation angle on small strain responses. *J. Geotech. Geoenviron. Eng.* **2012**, *138*, 526–534. [CrossRef]
8. Kim, S.; Finno, R. Inverse analysis of a supported excavation in Chicago. *J. Geotech. Geoenviron. Eng.* **2019**, *145*, 04019050. [CrossRef]
9. Kim, T.; Jung, Y.-H. Optimizing material parameters to best capture deformation responses in supported bottom-up excavation: Field monitoring and inverse analysis. *KSCE J. Civ. Eng.* **2022**, *26*, 3384–3401. [CrossRef]
10. Zhu, C.; Long, S.; Zhang, J.; Wu, W.; Zhang, L. Time series multi-sensors of interferometry synthetic aperture radar for monitoring ground deformation. *Front. Environ. Sci.* **2022**, *10*, 929958. [CrossRef]
11. Kim, T.; Jung, J.; Min, H.; Jung, Y.-H. An entropy analysis-based window size optimization scheme for merging LiDAR data frames. *Sensors* **2022**, *22*, 9293. [CrossRef]
12. Jiang, R.; Jáuregui, D.V.; White, K.R. Close-range photogrammetry applications in bridge measurement: Literature review. *Measurement* **2008**, *41*, 823–834. [CrossRef]
13. Luhmann, T. Close range photogrammetry for industrial applications. *ISPRS J. Photogramm. Remote Sens.* **2010**, *65*, 558–569. [CrossRef]
14. Yilmaz, H.M.; Yakar, M.; Gulec, S.A.; Dulgerler, O.N. Importance of digital close-range photogrammetry in documentation of cultural heritage. *J. Cult. Herit.* **2007**, *8*, 428–433. [CrossRef]
15. Remondino, F. Heritage recording and 3D modeling with photogrammetry and 3D scanning. *Remote Sens.* **2011**, *3*, 1104–1138. [CrossRef]
16. Fiorillo, F.; Limongiello, M.; Jiménez Fernández-Palacios, B. Testing GoPro for 3D model reconstruction in narrow spaces. *Acta IMEKO* **2016**, *5*, 64. [CrossRef]
17. Altuntas, C.; Hezer, S.; Kırlı, S. Image based methods for surveying heritage of masonry arch bridge with the example of Dokuzunhan in Konya, Turkey. *Sci. Cult.* **2017**, *3*, 13–20. [CrossRef]
18. Angelini, A.; Cozzolino, M.; Gabrielli, R.; Gentile, V.; Mauriello, P. Three-dimensional modeling and non-invasive diagnosis of a huge and complex heritage building: The Patriarchal Basilica of Santa Maria Assunta in Aquileia (Udine, Italy). *Remote Sens.* **2023**, *15*, 2386. [CrossRef]
19. Eltner, A.; Sofia, G. Structure from motion photogrammetric technique. In *Developments in Earth Surface Processes*; Elsevier: Amsterdam, The Netherlands, 2020; Volume 23, pp. 1–24, ISBN 9780444641779.
20. Dabove, P.; Grasso, N.; Piras, M. Smartphone-based photogrammetry for the 3D modeling of a geomorphological structure. *Appl. Sci.* **2019**, *9*, 3884. [CrossRef]
21. Stumpf, A.; Malet, J.-P.; Allemand, P.; Pierrot-Deseilligny, M.; Skupinski, G. Ground-based multi-view photogrammetry for the monitoring of landslide deformation and erosion. *Geomorphology* **2015**, *231*, 130–145. [CrossRef]
22. Gance, J.; Malet, J.-P.; Dewez, T.; Travelletti, J. Target detection and tracking of moving objects for characterizing landslide displacements from time-lapse terrestrial optical images. *Eng. Geol.* **2014**, *172*, 26–40. [CrossRef]
23. Demmler, C.; Adams, M.; Hormes, A. From UAV-photogrammetry to displacement rates-monitoring slope deformations in Alpine terrain. In Proceedings of the EGU General Assembly 2020, Online, 4 May 2020.
24. Sturzenegger, M.; Stead, D. Close-range terrestrial digital photogrammetry and terrestrial laser scanning for discontinuity characterization on rock cuts. *Eng. Geol.* **2009**, *106*, 163–182. [CrossRef]
25. Bales, F.B. Close-range photogrammetry for bridge measurement. *Transp. Res. Rec.* **1984**, *950*, 39–44.
26. Leitch, K.R. Close-Range Photogrammetry Measurement of Bridge Deformation: A Non-Contact Analysis Method. Ph. D. Thesis, New Mexico State University, Las Cruces, NM, USA, 2002.
27. Lee, H.; Han, D. Deformation measurement of a railroad bridge using a photogrammetric board without control point survey. *J. Sens.* **2018**, *2018*, 6851252. [CrossRef]
28. Ahn, Y.; Peterson, S.; Nazari, M. *Bridge Monitoring Using a Digital Camera: Photogrammetry-Based Bridge Dynamics Monitoring*; Mineta Transporation Institute: San Jose, CA, USA, 2019.
29. Lee, H.; Oh, J. 3D displacement measurement of railway bridge according to cyclic loads of different types of railcars with sequential photogrammetry. *Appl. Sci.* **2023**, *13*, 1359. [CrossRef]

30. Luhmann, T.; Robson, S.; Kyle, S.; Boehm, J. *Close-Range Photogrammetry and 3D Imaging*; De Gruyter: Berlin, Germany, 2019; ISBN 9783110607253.
31. McGuire, M.P.; Yust, M.B.S.; Shippee, B.J. Application of terrestrial lidar and photogrammetry to the as-built verification and displacement monitoring of a segmental retaining wall. In Proceedings of the Geotechnical Frontiers 2017, Orlando, FL, USA, 30 March 2017; American Society of Civil Engineers: Reston, VA, USA, 2017; pp. 461–471.
32. Balestrieri, E.; Daponte, P.; De Vito, L.; Lamonaca, F. Sensors and measurements for unmanned systems: An overview. *Sensors* **2021**, *21*, 1518. [CrossRef]
33. Patel, T.; Guo, B.H.W.; Van Der Walt, J.D.; Zou, Y. Effective motion sensors and deep learning techniques for unmanned ground vehicle (UGV)-based automated pavement layer change detection in road construction. *Buildings* **2022**, *13*, 5. [CrossRef]
34. Liu, O.; Yuan, S.; Li, Z. A survey on sensor technologies for unmanned ground vehicles. In Proceedings of the 2020 3rd International Conference on Unmanned Systems (ICUS), Harbin, China, 27 November 2020; pp. 638–645. [CrossRef]
35. Guastella, D.C.; Cantelli, L.; Melita, C.D.; Muscato, G. A global path planning strategy for a UGV from aerial elevation maps for disaster response. In Proceedings of the 9th International Conference on Agents and Artificial Intelligence, Porto, Portugal, 24–26 February 2017; pp. 335–342. [CrossRef]
36. Bonadies, S.; Lefcourt, A.; Gadsden, S.A. A Survey of Unmanned Ground Vehicles with Applications to Agricultural and Environmental Sensing. In Proceedings of the Autonomous Air and Ground Sensing Systems for Agricultural Optimization and Phenotyping, Baltimore, MD, USA, 17 May 2016; 98660Q. Valasek, J., Thomasson, J.A., Eds.; SPIE: Baltimore, MD, USA, 2016; Volume 9866. [CrossRef]
37. Professional Photogrammetry and Drone Mapping Software. Available online: https://www.pix4d.com/ (accessed on 5 May 2023).
38. *ISO 17123-2:2001*; Optics and Optical Instruments—Field Procedures for Testing Geodetic and Surveying Instruments—Part 2: Levels. ISO: Geneva, Switzerland, 2001.